Effectiveness of Cavity Shielding in the LCLS-II Cryomodule

Y. Orlov and I. Terechkine

Introduction.

During the early stages of the LCLS-II cryomodule shielding studies, it was shown that there exist several options of building a magnetic shield that can bring the residual magnetic field to the required average level of ~3 mG in the presence of the earth magnetic field. In the studies this field was described by two components: the longitudinal (200 mG) and the vertical (500 mG) [1]. It was also shown that no solution to the problem exists without using a set of coils along the cryomodule installed to compensate the longitudinal component of the earth field. This component was found to interact unfavorably with the vacuum vessel, made of steel and serving as a primary magnetic shield, and with the secondary magnetic shield made of Cryoperm-10 material. The reason of this was that both the primary and the secondary shields have fairly high aspect ratios. Longitudinal cross-section through the cavity in Fig. 1 gives an idea of the secondary sheild design. It is a two-layer shield; the first (inner) layer is made just outside the LHe vessel of the cavity and equipped with an end cup to simplify installation of a tuner and of an RF coupler. The second layer is introduced mainly to reduce the impact of the transverce component of the earth field, which became the main concern after the compensating coils reduced the level of the longitudinal component. The cavity is located 247 mm below the axis of the cryovessel, which is ~1 m in diameter.

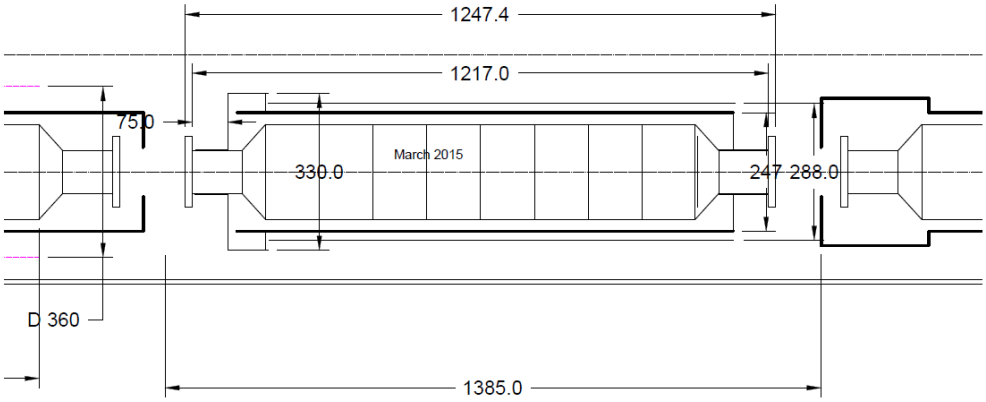

Fig. 1. Simplified scheme of the secondary shield.

Although a proof-of-principle modeling, which used the simplified configuration of the environmental magnetic field and the simplified design of the magnegtic shield, provided some degree of confidence that the goal of getting the desired level of the magnetic field is within the reach, it did not take into account multiple technological openings in the layers of the shield that came into existence during the design stage. Some of the openings could be easily protected by using auxiliary side shielding, but making simular arrangements for others could result in significant complications in the design of the shielded cavity. Several iterations of the shield design were made before the current version of the shield was proposed [2]. Some details of the two-layer secondary magnetic sheild design are shown in figures below.

Verification of the magnetic shield design.

Fig. 2 shows the location of the end cup attached to the inner layer of the shield. The end cup was introduced at the location of the first cell of the cavity to add additional magnetic protection in the presence of the tuning block installed nearby (not shown in the picture). The start of the cup corresponds to the longitudinal coordinate where the raduis of the shell in the first cell of the cavity is maximum.

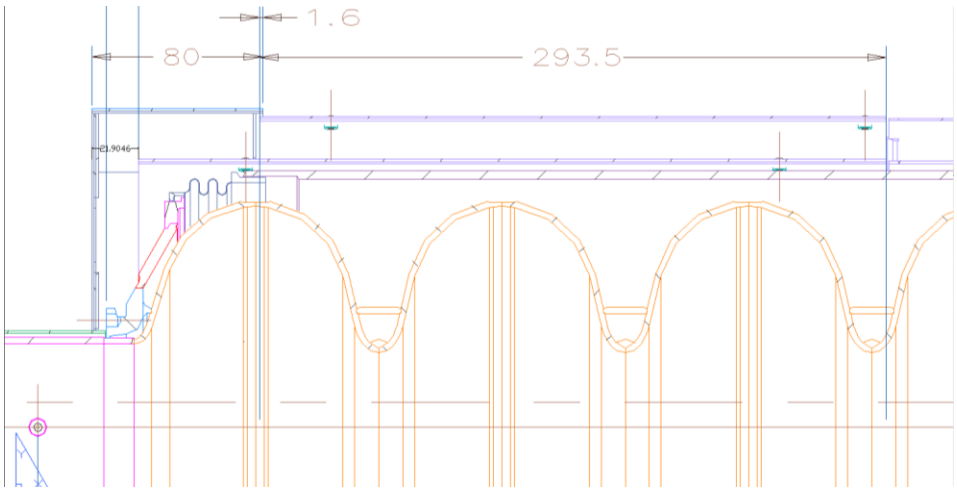

Fig. 2. The end cup of the secondary shield.

Fig. 3 shows the location and the size of the pick-up and the coupler flanges of the cup side of the cavity. The beam pipe and the technological openings are protected by auxiliary local shielding. The presence of the flanges requires making several cuts in the end wall of the cup.

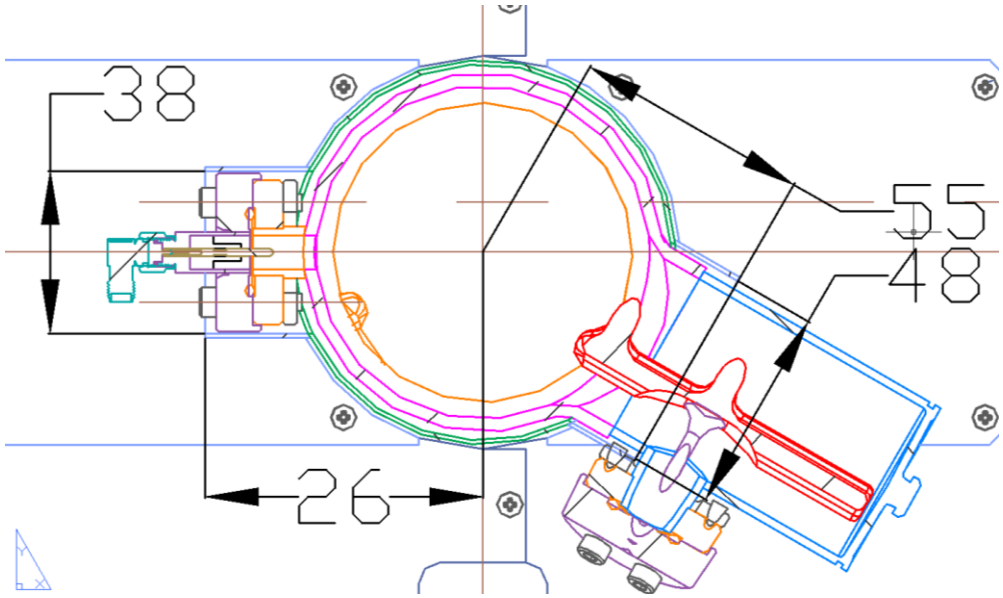

Fig. 3. Box side technological piping arrangement

Fig. 4 and 5 show the implementation of the far end of the cavity, where the presence of flanges also requires making cuts through the end plate of the magnetic shield.

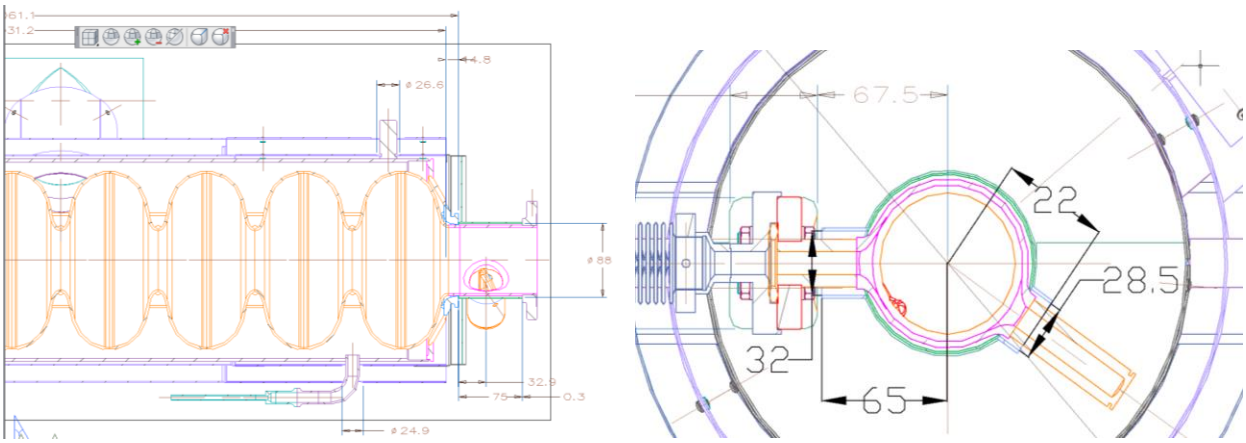

Fig. 4. Far end of the cavity assembly. Auxiliary magnetic shield is installed around the beam pipe and the side pipes.

In Fig. 5 cavity support bars are shown that require making corresponding cut-offs both in the first and the second layer of the shield.

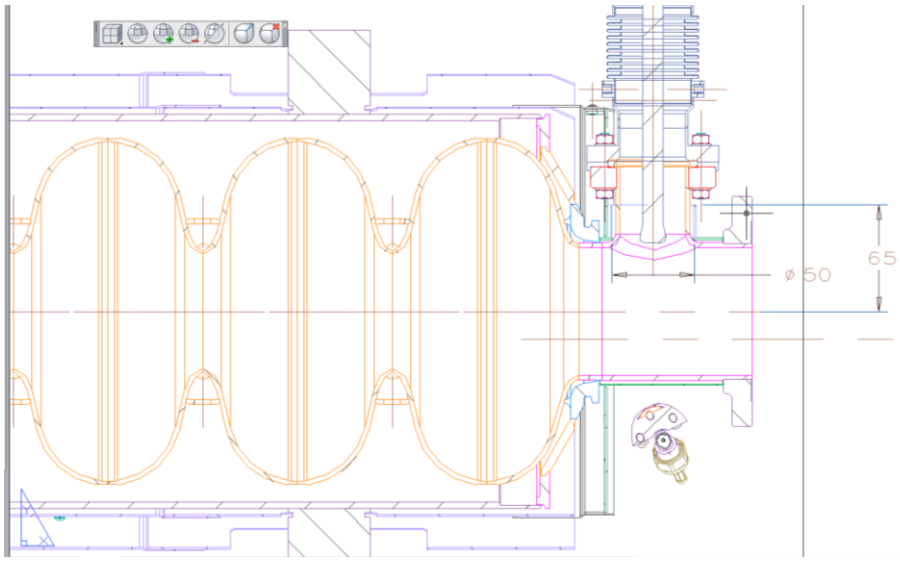

Fig. 5. Far end of the cavity assembly. Magnetic shield surrounds the beam pipe and the high order mode coupler. Support bars are seen near the middle cell in the picture. Corresponding cut-offs are made in walls of the first and the second layers of the shield.

Fig. 6 shows a cross-section through the exshaust pipe of the LHe vessel. This pipe is protected by the magnetic shield connected to the second layer of the secondary shield.

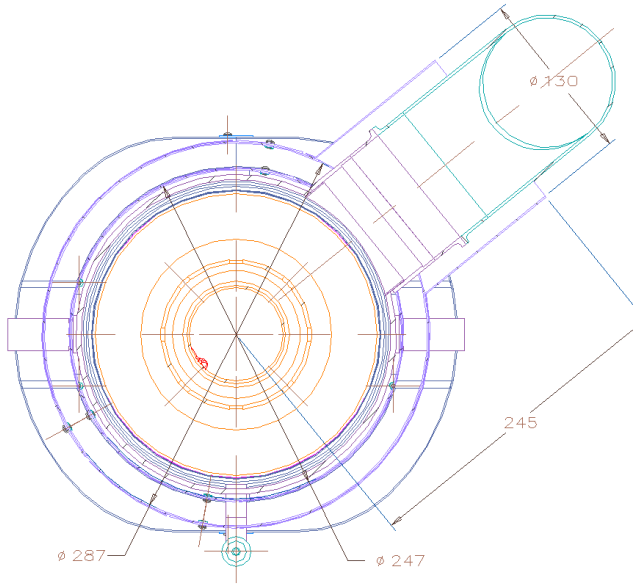

Fig. 6. LHe exshaust pipe with additional protective shield.

Having so many features oriented not only in the horizontal and vertical planes forces us to use (during the verification modeling) the environmental magnetic field that is close to what is expected at the location where the cryomodules will be used. Corresponding field map was measured at SLAC and was provided for this study by A.C. Crawford. For the purpose of this study, the environmental magnetic field can be specified as the following: the longitudinal component B_X = 0.15 G, the vertical component B_Z = 0.25 G, and the transverce horizontal component B_Y = 0.5 G.

The two-layer shield geometry was implemented in COMSOL; all technological holes in the layers of the shield were added. Examples of the implementation are shown in Fig. 7 and Fig. 8.

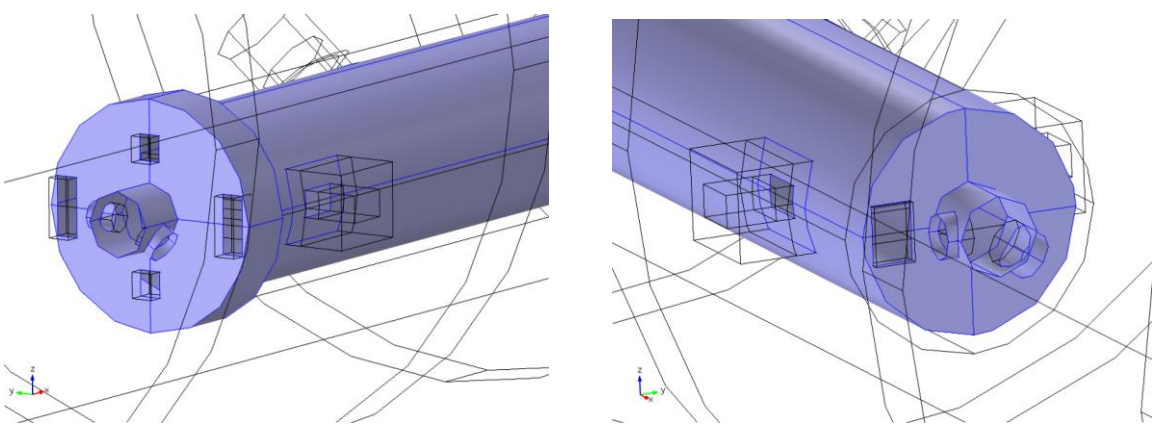

Fig. 7. The first layer of the secondary magnetic shield

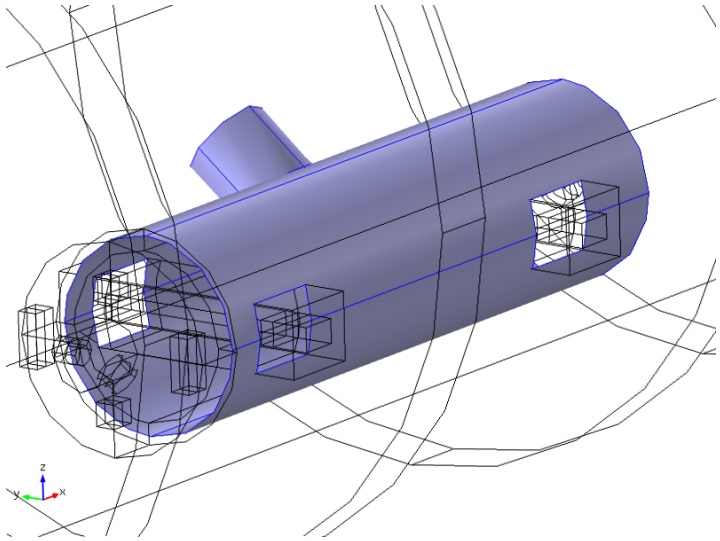

Fig. 8. The second layer of the secondary magnetic shield

The current in the compensating coils was set to compensate the longitudinal component of the magnetic field B_X = 150 mG.

Graphs of magnetic field inside the two-layer secondary shield with all technological holes in accordance with the current design are shown in Fig. 9. The traces of the field are along straight lines at different radii (35 mm and 90 mm) and at different planes marked by their azimuth angle "Phi". E.g. the azimuth angle Phi39 of the plane that goes though the LHe exhaust pipe in Fig. 6 is 39º from the horizontal plane.

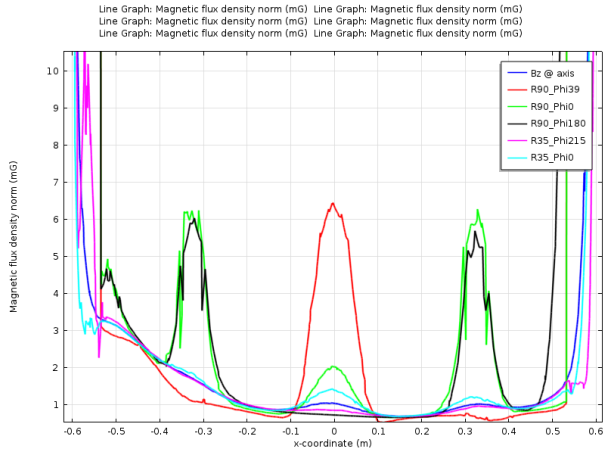

Fig. 9. Magnetic field inside the secondary shield along the lines at different radiuses and azimuths.

One can see increased level of the magnetic field on walls of the cavity at the locations closest to the openings on the magnetic shield. This set of curves serves as a reference when sources of magnetic flux are added outside and inside the secondary shield to check on their impact in [4]. The start of the first cell is at X ≈ -0.544 m; the end of the last cell is at X = 0.5 m. The planes where corresponding cells have the maximum radius are ~58 mm inward.

Expansion of the environmental magnetic field compensation concept.

As the longitudinal component of the earth magnetic field is significantly reduced inside the cryomodule by employing the compensating coils, the Y and Z components of the environmental magnetic field become the main sources of the undesired field inside the secondary magnetic shield. The outer layer of the secondary shield was introduced entirely for shunting these two transverse field components. As an alternative option, the field compensation concept can be applied. For simple verification of this possibility, we can use layers with currents; similar results are expected if a system of coils is used. To compensate the vertical component, current loop with the length L = 7 m and height and width of 2 m is used. Surface current density in this loop is 80 A/m. To compensate the transverse component, current loop with the length L = 6 m and height and width of 1.5 m is used. Surface current density in this loop is 40 A/m. As a result, we get the distribution of the magnetic field shown in Fig. 10.

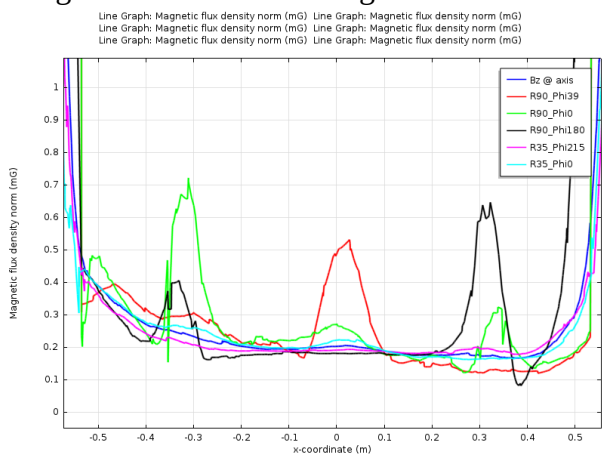

Fig. 10. Magnetic field inside the secondary shield after the vertical and the transverse field components are compensated.

With the use of the second layer shielding, the field in the cavity becomes less than 1 mG. Field maps in the exhaust pipe plane and in the horizontal plane are shown in Fig. 11.

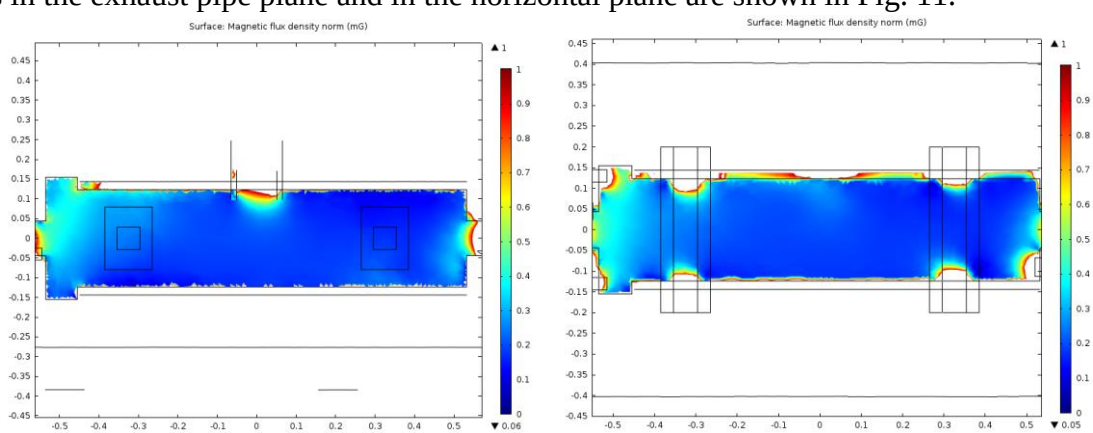

a) b)

Fig. 11. Magnetic field map in the exhaust pipe plane (a) and in the horizontal plane (b).

One can see that the magnetic field inside the secondary shield can be significantly reduced if the logic of using the compensation is fully explored.

Impact of magnetized elements installed on the cavity suspension bars.

In [3], a simplified way to evaluate magnetic field generated by magnetized objects was suggested that used the magnetic momentum quantity as a starting point. According to this approach, the field can be calculated using the following expression:

$$B(z) = m/(2\pi z^3)$$

The magnetic momentum *m* can be found by using:

$$m = B_r \cdot V$$

where B_r is the remnant magnetic field and V is the volume of the object.

We can use this approach to evaluate the magnetic field generated by the rollers of linear bearings installed around the support bars of the cavity shown in Fig. 5. As the rollers are installed in close vicinity of the rectangular cut-offs in the layers of the shielding, the field generated by the magnetized bearings has easy access inside the guarded space.

Schematic drawing of the bearing is shown in Fig. 12. The case (1) and the separator (2) are made of Aluminum 6061-T6 alloy, which is non-magnetic. The needles of rolling bearings (3) are made of 316 stainless steel; their diameter is 3.0 mm and the length is 13.8 mm. Six needles spaced by 6 mm are used in one set of rollers. Three sets of rollers are installed at each end of the support bar.

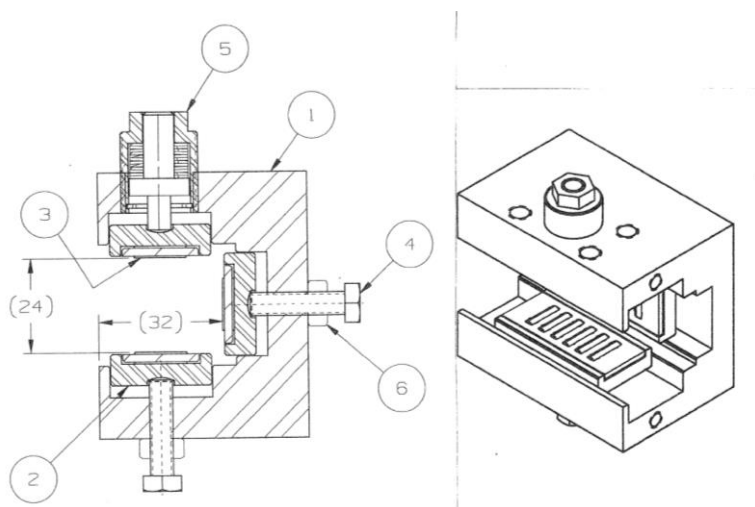

Fig. 12. Linear bearings assembly

In accordance with what was found in [4], let's assume that the remnant flux density of 316 steel is 0.5 G and the permeability of the material is 1.0. Then expected magnetic moment of one needle is

$$B_r \cdot V = \pi/4 \cdot d^2 \cdot l \cdot B_r = 5 \cdot 10^{-12}\ T \cdot m^3$$

Let's assume that all the needles are magnetized in the same direction and that the total magnetic moment of all 18 needles in one roller is $m = 1 \cdot 10^{-10}\ T \cdot m^3$. With this moment, the field at the distance 50 mm from the center of the magnetic dipole is

$$B_{50mm} = m/(2\pi \cdot z^3) = 10^{-10}/(2\pi \cdot 125 \cdot 10^{-6}) \approx 1.3\ mG.$$

This level of the magnetic field increase does not seem significant in comparison with the base level in Fig. 9. In the presence of the shield, this small level may be even smaller.

To verify this evaluation, a modeling was made where one cylinder was used with the total magnetic moment m = 10^{-10} T·m^3 placed in the center of the bearing assembly. This magnetic moment was introduced by assigning a 10 G residual field in the material. Fig. 13 compares the field graphs corresponding to the cases without (a) and with (b) the magnetized cylinder.

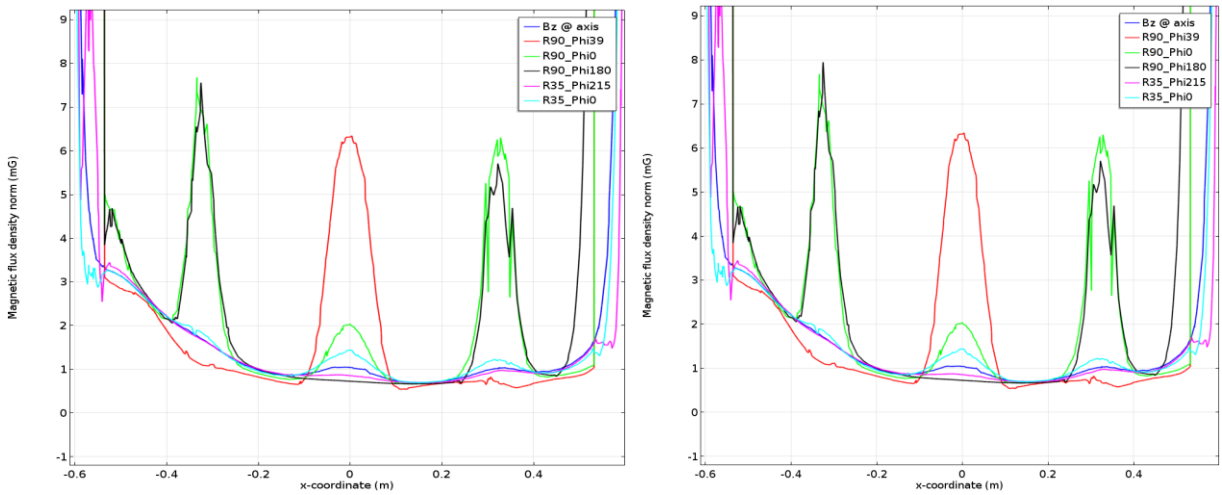

a) b)

Fig. 13. Magnetic field without (a) and in the presence (b) of a 10^{-10} T·m^3 magnetic moment

One can see the increase of the field of ~0.5 mG at the location Phi = 180^0, which is where the magnetized cylinder was placed. As expected, due to the presence of the shield this value is smaller than evaluated earlier using the simplified expression. Using the real geometry with 18 needles oriented as shown in Fig. 12 results in a very similar modeling output shown in Fig. 14.

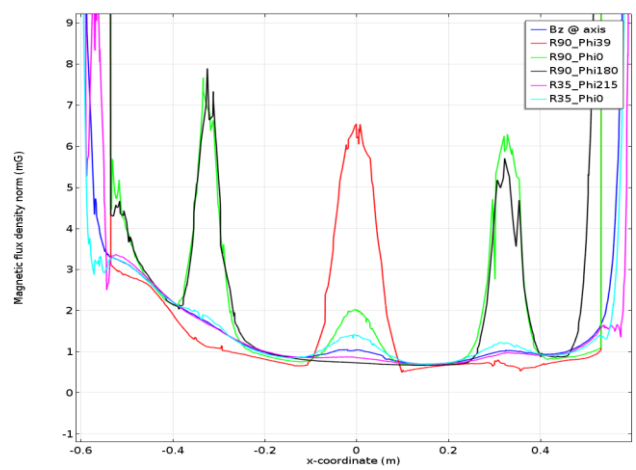

Fig. 14. Magnetic field from the magnetized roller needles located in accordance with Fig. 12

Comparing Fig. 14 and Fig. 13-b, one can conclude that the using simple geometry with the total magnetic momentum of the assembly results is justified - no significant difference of the expected added magnetic field is seen when the sum of all magnetic moments is used to make simple evaluation instead of using real geometry during the modeling.

It is tempting to understand what can happen if hardened steel needles are used instead of those made of 316 steel. Let's assume $B_r \approx 5000$ G and $H_c \approx 25$ Oe, making the effective permeability in the demagnetizing branch of the magnetization curve $\mu_{eff} \approx 200$. In this case, the field near the surface of the cavity far exceeds the 10 mG limit for the local field inside the shield; it reaches ~50 mG. Fig. 15 shows corresponding graphs and a field map; as earlier, the direction of magnetization for all the needles was the same.

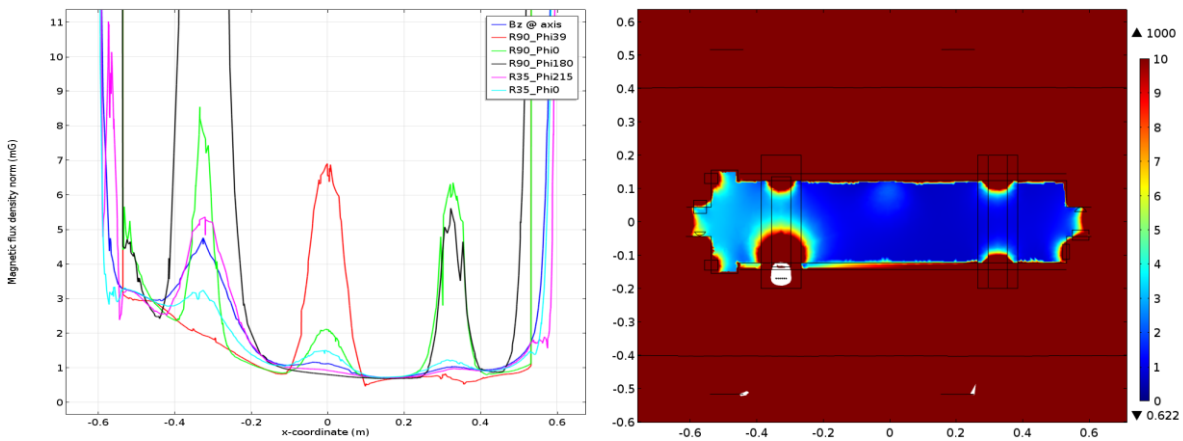

Fig. 15. Magnetic field graphs and map for the case of correlated magnetization of hardened steel roller needles.

In this case, demagnetization process can solve the problem as, in accordance with findings made in [4], the residual magnetic field after a secondary magnetization in a weak field will not exceed ~10 G.

Conclusion:

1. Shielding of the environmental magnetic field to the level not exceeding ~10 mG seems feasible using suggested shield design and longitudinal field compensating coils.
2. Using additional sets of coils for compensation of the transverse components of the magnetic field will lead to even better shielding effectiveness with the expected level of field on the cavity walls below 1 mG. Using this approach, significant simplification of the secondary magnetic shielding design is possible.
3. Sets of roller bearings installed in the vicinity of the openings in the shielding around the cavity support bars can increase the field on the cavity walls above the safe level if the rollers are made of hardened steel and magnetized. Demagnetization is a solution in this case as well as using non-magnetic or weakly magnetic (like 316) alloys.

References:

1. I. Terechkine, “Some Options for Improving the Effectiveness of Magnetic Shielding in the LCLS-II Cryomodule”, FNAL TD note TD-14-006, November 2014.
2. Y. Orlov, Team Center document # ????.
3. I. Terechkine, “Magnetic Field of Magnetized Ellipsoids”, FNAL TD note TD-15-006, June 2015.
4. A.C. Crawford and I. Terechkine, “Impact of Material Magnetization on the Magnetic Field inside LCLS Cryomodule”, FNAL TD note TD-15-006, June 2015.